URSI GASS 2023, Sapporo, Japan, 19 – 26 August 2023

Experimental Evaluation of Forward and Inverse Solvers for Metasurface Design

Mario Phaneuf*, Max Kelly, and Puyan Mojabi
University of Manitoba, Winnipeg, Canada; contact e-mail: phaneuf3@myumanitoba.ca

Abstract

Electromagnetic forward and inverse solvers are considered for the analysis and design of electromagnetic metasurfaces. This paper reviews (i) a forward solver that takes the surface susceptibilities of metasurfaces and calculates their scattered fields and (ii) an inverse solver that takes user-defined desired power patterns and outputs the required metasurface properties. An omega-bianisotropic transmitting metasurface is then fabricated and measured to evaluate the performance of these forward and inverse solvers.

1 Introduction

Electromagnetic (EM) engineering problems can broadly be classified as *forward* problems or *inverse* problems. In forward problems, we aim to calculate the output of a known system when excited by a known input. For example, the calculation of an antenna's unknown far-field radiation pattern (output), given the known properties of the antenna structure (system) and its feeding structure (input), would be classified as a forward problem. In EM inverse problems, the opposite is generally true, i.e., the output of the system is known, and we wish to infer the properties of the now unknown system or input to the system, or both. EM inverse problems are usually associated with imaging and characterization applications where the output of the system is known through measurements of the system output. Alternatively, EM inversion techniques can be applied to design problems where the output is taken to be the user-defined performance criteria of the system to be found. This procedure, which is sometimes referred to as inverse design, takes the desired output specifications and then *inverts* these to determine the required system characteristics needed to achieve the design. It is important to note that solving inverse problems may require solving forward problems as a means to evaluate the fit of an estimated solution. If an iterative algorithm is used, this information can then be used to produce the next estimate of the solution. Thus, while forward and inverse problems are distinctly defined, their usage is not mutually exclusive and can often be applied to the same engineering problem.

Herein, we focus on forward and inverse solvers for EM metasurface analysis and design. *Metasurfaces* are thin artificial materials that can systematically transform EM waves by the proper design of their sub-wavelength unit cells. The transformation can consist of reflected or transmitted waves (or both) with respect to incident EM waves which impinge on the metasurface; this has seen usage in a myriad of different EM engineering applications, such as smart radio environments [1]. The metasurface unit cells provide the functionality of the metasurface by giving rise to electric and magnetic surface polarization densities, which, when converted to equivalent surface electric and magnetic currents, support the required discontinuities in the electric and magnetic fields and thus enable the desired wave transformation(s). Although metasurfaces are electrically thin with sub-wavelength unit cells, their aperture size is electrically large; hence, they are multi-scale structures. Since the full-wave simulation of these multi-scale structures is computationally expensive, it is important to develop fast forward solvers that can predict the general performance of the metasurfaces. This is particularly the case when using an iterative design procedure that requires the forward problem to be solved many times. The forward solver considered herein is known as the implicit IE-GSTC solver [2]. This method utilizes an integral equation (IE) approach in conjunction with the metasurface boundary conditions known as the generalized sheet transition conditions (GSTCs) [3]. Similar to forward solvers such as [4, 5], the use of the GSTCs removes the necessity to simulate the whole metasurface (in our case, three-layered patterned metallic claddings over two layers of dielectric substrates [6]); instead, we are able to abstract the effect of the embedded metallic traces into homogenized surface susceptibilities. Given the surface susceptibilities of each unit cell and the incident field impinging on the metasurface, the implicit IE-GSTC method calculates the fields scattered by the metasurface. On the other hand, the inverse solver used herein relies on an inverse source algorithm [7, 8] that finds the required surface susceptibilities from the knowledge of the desired performance criteria and the incident field.

2 Forward Metasurface Solver

For ease of manufacturing, the metasurface considered in this paper is planar. In addition, we assume that the metasurface does not change along its vertical axis and that the corresponding height of the metasurface is sufficiently large such that we can consider the fields in the centered azimuth

plane to be under a quasi two-dimensional (2D) scenario. A visualization of the 2D problem is shown in Fig. 1. The metasurface, which is located on the plane $\mathscr{M}$, separates the problem into two regions: Region 1, which contains the incident field impinging upon the metasurface and the reflection from the metasurface (if applicable); and Region 2, which contains the transmitted field. Due to the 2D assumption, the metasurface properties are assumed to be non-variant along the z direction. We further assume that the fields are transverse-magnetic (TM; H_z component only). In addition, a time dependency of $\exp(j\omega t)$ is considered where $j^2 = -1$, ω is the angular frequency, and t denotes time. Finally, μ_0 and ε_0 are the free-space permeability and permittivity respectively.

The implicit IE-GSTC forward solver [2] finds the scattered fields of a metasurface by utilizing IEs and modeling the metasurface with the GSTCs. This forward solver is functionally similar to other IE-GSTC solvers [4, 5], but differs in its formulation [2] in an attempt to reduce the number of fundamental unknowns. The GSTCs relate the change in the tangential fields across the metasurface, denoted by $\Delta\vec{\Psi}$ where $\vec{\Psi} \in \{\vec{E}, \vec{H}\}$, to the average fields across the metasurface, denoted by $\vec{\Psi}_{\text{av}}$, and the surface susceptibilities of the metasurface denoted by χ [3]. The fields in the GSTCs can then be broken into the incident and scattered fields. Noting the zero-thickness assumption associated with the utilized GSTCs, the incident field on both faces of the metasurface will be the same; thus, $\Delta\vec{\Psi} = \Delta\vec{\Psi}^{\text{scat}}$ and $\vec{\Psi}_{\text{av}} = \vec{\Psi}^{\text{scat}}_{\text{av}} + \vec{\Psi}^{\text{inc}}$. We can then obtain two equations for the equivalent surface electric $\vec{J}^{\text{eq}}$ and magnetic $\vec{K}^{\text{eq}}$ currents that support $\Delta\vec{\Psi}^{\text{scat}}$ and thus radiate the same scattered fields emanating from the metasurface. These equations relate $\vec{J}^{\text{eq}}$ and $\vec{K}^{\text{eq}}$ to $\vec{\Psi}^{\text{scat}}_{\text{av}}$ (unknown), χ (known), and $\vec{\Psi}^{\text{inc}}$ (known). The key feature of the implicit IE-GSTC solver is the following: if $\vec{J}^{\text{eq}}$ and $\vec{K}^{\text{eq}}$ are passed to the electric and magnetic field IE operators, denoted by $\mathscr{L}$ and $\mathscr{K}$ respectively [9], and then evaluated at the observation point $\vec{r}$ on the surface $\mathscr{M}$, the principal values (pv) of these integrals yield the average scattered fields [10], i.e.,

$$\vec{H}^{\text{scat}}_{\text{av}}(\vec{r}) = [-j\omega\varepsilon_0(\mathscr{L}\vec{K}^{eq})(\vec{r}) + (\mathscr{K}\vec{J}^{\text{eq}})(\vec{r})]_{\text{pv}}, \quad (1)$$

$$\vec{E}^{\text{scat}}_{\text{av}}(\vec{r}) = [-j\omega\mu_0(\mathscr{L}\vec{J}^{\text{eq}})(\vec{r}) - (\mathscr{K}\vec{M}^{\text{eq}})(\vec{r})]_{\text{pv}}. \quad (2)$$

Substituting the aforementioned expressions of $\vec{J}^{\text{eq}}$ and $\vec{K}^{\text{eq}}$ in terms of $\vec{\Psi}^{\text{scat}}_{\text{av}}$, χ, and $\vec{\Psi}^{\text{inc}}$ in (1) and (2), we can then solve for the unknown $\vec{\Psi}^{\text{scat}}_{\text{av}}$, and then trivially obtain $\vec{J}^{\text{eq}}$ and $\vec{K}^{\text{eq}}$. Finally, we can calculate the total fields everywhere by re-radiating $\vec{J}^{\text{eq}}$ and $\vec{K}^{\text{eq}}$ and augmenting the result by the incident field [2].

3 Inverse Metasurface Solver

The utilized inverse solver takes a desired power pattern (a phaseless quantity), and then formulates a phaseless data misfit cost functional which is optimized to yield the required equivalent electric and magnetic currents of the metasurface to be designed. Appropriate regularization terms are also added to this data misfit cost functional to favor lossless and passive designs with relatively smooth variations in equivalent currents (via local power conservation at each metasurface unit cell [6] and total variation regularizers [11]). Once this overall cost functional is minimized, the equivalent currents can be found and the required surface susceptibilities of the metasurface can be inferred. The details of the implementation can be found in [7, 8].

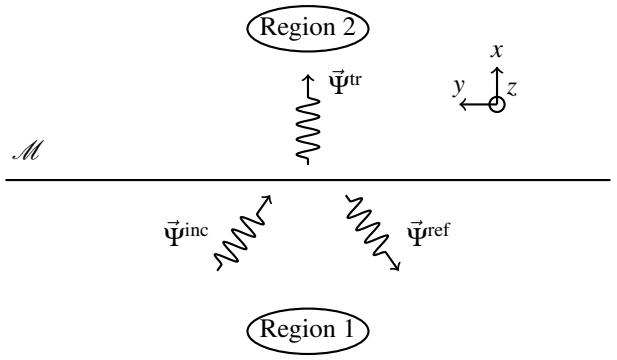

Figure 1. The metasurface on the plane $\mathscr{M}$ is parallel to the yz plane and separates the 2D problem ($\partial/\partial z = 0$) into Region 1 and Region 2 with incident, reflected (if applicable), and transmitted fields $\vec{\Psi} \in \{\vec{E}, \vec{H}\}$. Adapted from [2].

4 Copper Trace Design

After the inverse solver yields the required surface susceptibilities, these must next be converted to the physically realizable unit cells. As will be seen in the next section, we modify the beam of a normally incident plane when passing through the metasurface while simultaneously aiming to minimize the reflections from the metasurface. Thus, we rely on omega-bianisotropic metasurfaces [6] to provide sufficient degrees of freedom to achieve this objective. The unit cells of this type of metasurface can be implemented by two substrate layers supporting three cascaded layers of copper metallic claddings. The three-layered copper traces are in the form of "dog-bones" [12] and are realized by printed circuit board fabrication. As the dielectric substrate, we choose Rogers RO3010 with a thickness of 1.27 mm and a relative permittivity of 10.2. To bond the two substrate layers, we use Rogers 2929 bondply with a thickness of 0.076 mm. For each unit cell, the associated scattering matrix for a particular choice of dog-bone dimensions can be found through a full-wave simulation (Ansys HFSS in this case). By iteratively modifying the dimensions, a lookup table can be formed which relates these dimensions to its scattering matrix. Finally, we use this lookup table to relate the desired scattering parameters (which can be calculated from the surface susceptibilities) to the realizable unit cells. In particular, we focus on the forward scattering parameter which is most relevant for reciprocal and reflectionless metasurfaces. The overall metasurface is then further optimized in HFSS for improved performance. The scattering parameters of the unit cells are used to infer the surface susceptibilities that will be used in the forward solver.

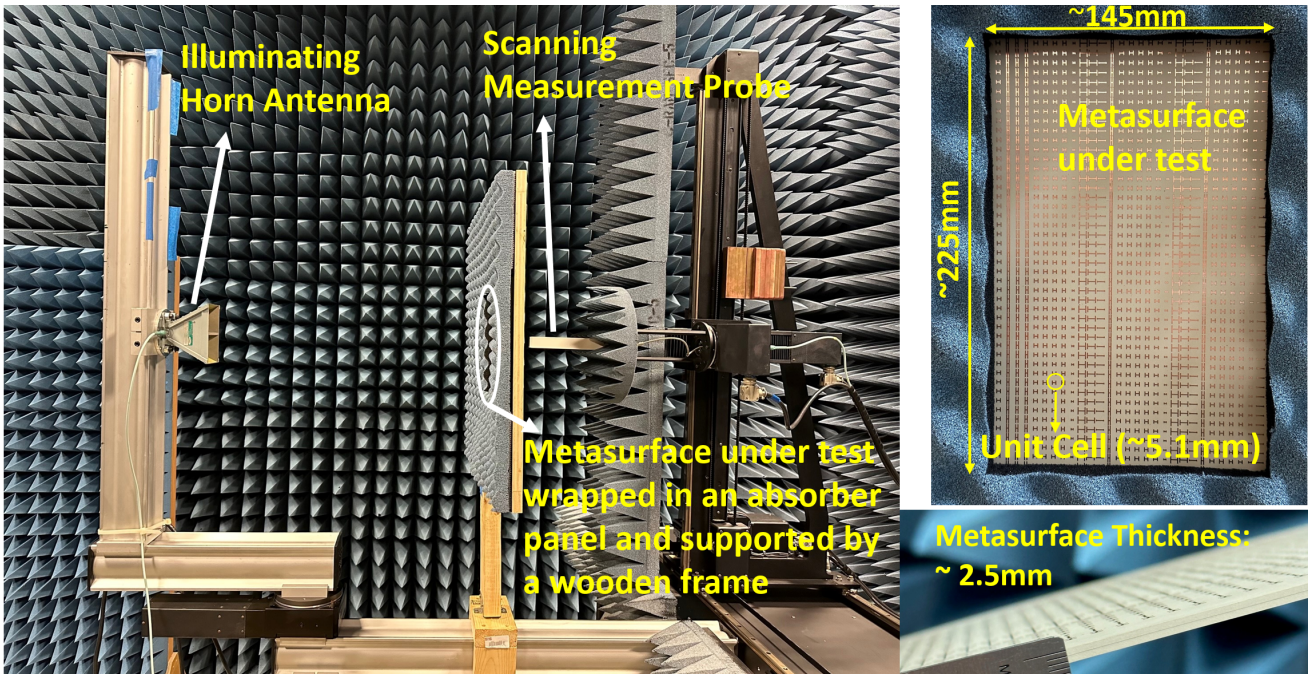

Figure 2. (**Left**) The metasurface under test in a planar near-field antenna range. The horn antenna illuminates the metasurface at a distance of roughly 60 cm from the input face of the metasurface. An open-ended waveguide probe on the other side of the metasurface records the near-field data on the measurement plane. The probe is about 8.5 cm away from the output face of the metasurface and its scan plane is 45 cm $\times$ 45 cm. The spatial sampling resolution of the probe is about 0.8 cm in both the horizontal and vertical scans. (**Right, top**) Dimensions of the metasurface. (**Right, bottom**) Metasurface thickness.

5 Results

The metasurface under test is designed by the inverse solver to transform a normally incident plane wave into fields which produce a desired power pattern with minimal reflections at 10.5 GHz.[1] The EM measurements of this metasurface were performed using a planar near-field (NF) measurement system shown in Fig. 2. The resultant fields close to the output of the metasurface were collected by a waveguide probe. The measurement software then obtains the far-field (FF) pattern (azimuth plane) through a NF to FF transformation. The measured power pattern is shown in Fig. 2 along with the HFSS simulation of the actual three-layered patterned copper claddings and the implicit IE-GSTC result of the corresponding susceptibility model.[2] In order to better interpret these results, Table 1 shows the following performance characteristics: half-power beamwidth (HPBW), main beam angle, and the maximum side lobe level (SLL). As can be seen, the simulated and measured values vary slightly but are reasonably close to the desired values with the measured SLL being the most different.

To explain these discrepancies, we first highlight some sources of error in the experimental result, namely (i) NF system alignment errors, (ii) non-planar wavefront of the horn antenna (the inverse solver has assumed an incident plane wave), and (iii) multiple reflections between the probe and the metasurface. In addition, the inverse solver may not be able to fully achieve the desired power pattern as it needs to account for other constraints to implement the metasurface with lossless and passive elements. In addition, the surface susceptibilities fed into the forward solver are derived by considering each unit cell in a fully periodic environment. This relies on the quasi-periodicity assumption which is not completely valid; Fig. 2 shows that the metasurface is not periodic in the horizontal direction. Moreover, since our metasurface does not use any loss or gain mechanisms, it requires appropriate auxiliary surface waves [14] to properly tailor the field amplitude on the metasurface aperture to fully control the SLLs; thus, tailoring the SLLs is more challenging than steering the beam. Finally, as will be described at the conference, the least accurate result is the power transmission efficiency, defined as the ratio of the normal real power leaving the metasurface to that entering the metasurface. The HFSS simulation predicts an efficiency of about 73% whereas the forward solver predicts 85%. We speculate that this discrepancy is due to the presence of evanescent waves. Since these can propagate along the metasurface, the loss tangent of the RO3010 substrates will play a more significant role than what is embedded in the surface susceptibility model. (This explanation is supported by [14].) On the other hand, the measured result gives a transmission efficiency of about 57%. This is partly due to the fact that some of the unit cells are covered by the absorber and also the deviation of the horn illumination from an ideal plane wave.

[1] The desired pattern is obtained from the power pattern of an array of line sources and is the same as the desired power pattern used in [13].

[2] The measured result is reported at 10.3 GHz as we had a -0.2 GHz frequency shift as compared to the design frequency.

Characteristic	Des	IE-GSTC	Meas	HFSS
HPBW	13.9°	14.4°	14.0°	14.1°
Beam Angle	−35.0°	−34.7°	−36.2°	−36.0°
SLL_{max} dB	−12.9	−10.1	−7.07	−8.69

Table 1. Performance characteristics for inverse metasurface design ("Des" corresponds to the desired metasurface design and "Meas" corresponds to the measured data).

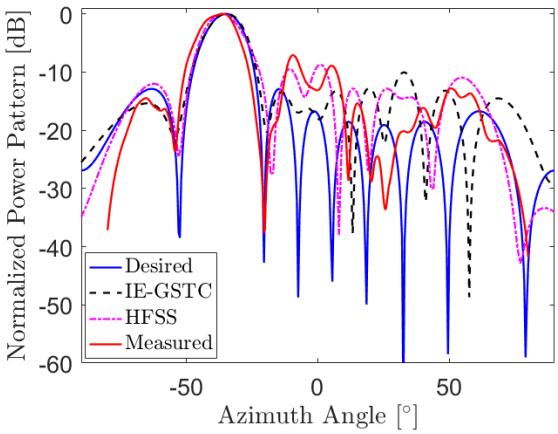

Figure 3. Normalized power patterns under four scenarios. The measured data cannot span the whole angular range due to the critical angle associated with planar NF systems.

6 Conclusion

We can conclude that the implicit IE-GSTC is useful for finding the angle and HPBW of main beams, and perhaps the initial side lobes. For more accurate results, particularly in the case of the power transmission efficiency, we should rely on measurements or full-wave simulations. However, this forward solver remains useful since it can provide a fast evaluation of the general performance of the metasurface, which is relevant for the situations outlined in the introduction. Similarly, the inverse solver in conjunction with the copper trace design approach was able to implement a metasurface that reasonably meets the overall desired specifications, except for the transmission efficiency.

References

[1] M. Di Renzo, A. Zappone, M. Debbah, M.-S. Alouini, C. Yuen, J. de Rosny, and S. Tretyakov, "Smart radio environments empowered by reconfigurable intelligent surfaces: How it works, state of research, and the road ahead," *IEEE J. Sel. Areas Commun.*, vol. 38, no. 11, pp. 2450–2525, 2020.

[2] M. Phaneuf and P. Mojabi, "An implicit IE-GSTC metasurface forward solver," in *URSI Int. Symp. Electromag. Theory (Submitted; Available online at TechRxiv preprint server)*, Canada, May 2023.

[3] K. Achouri, M. A. Salem, and C. Caloz, "General metasurface synthesis based on susceptibility tensors," *IEEE Transactions on Antennas and Propagation*, vol. 63, no. 7, pp. 2977–2991, 2015.

[4] M. Dehmollaian, N. Chamanara, and C. Caloz, "Wave scattering by a cylindrical metasurface cavity of arbitrary cross section: Theory and applications," *IEEE Transactions on Antennas and Propagation*, vol. 67, no. 6, pp. 4059–4072, 2019.

[5] T. J. Smy, V. Tiukuvaara, and S. Gupta, "IE-GSTC metasurface field solver using surface susceptibility tensors with normal polarizabilities," *IEEE Trans. Antennas Propag.*, vol. 70, no. 6, pp. 4752–4765, 2022.

[6] A. Epstein and G. V. Eleftheriades, "Arbitrary power-conserving field transformations with passive lossless omega-type bianisotropic metasurfaces," *IEEE Transactions on Antennas and Propagation*, vol. 64, no. 9, pp. 3880–3895, 2016.

[7] T. Brown, C. Narendra, Y. Vahabzadeh, C. Caloz, and P. Mojabi, "On the use of electromagnetic inversion for metasurface design," *IEEE Trans. Antennas Propag.*, vol. 68, no. 3, pp. 1812–1824, 2020.

[8] T. Brown, Y. Vahabzadeh, C. Caloz, and P. Mojabi, "Electromagnetic inversion with local power conservation for metasurface design," *IEEE Antennas Wireless Propag. Lett.*, vol. 19, no. 8, pp. 1291–1295, 2020.

[9] W. C. Gibson, *The method of moments in electromagnetics*, 2nd ed. Boca Raton, FL: CRC Press/Taylor & Francis Group, 2015.

[10] G. Hsiao and R. Kleinman, "Mathematical foundations for error estimation in numerical solutions of integral equations in electromagnetics," *IEEE Trans. Antennas Propag.*, vol. 45, no. 3, pp. 316–328, 1997.

[11] T. Brown and P. Mojabi, "Cascaded metasurface design using electromagnetic inversion with gradient-based optimization," *IEEE Trans. Antennas Propag.*, vol. 70, no. 3, pp. 2033–2045, 2022.

[12] G. Lavigne, K. Achouri, V. S. Asadchy, S. A. Tretyakov, and C. Caloz, "Susceptibility derivation and experimental demonstration of refracting metasurfaces without spurious diffraction," *IEEE Trans. Antennas Propag.*, vol. 66, pp. 1321–1330, 2018.

[13] M. Kelly, T. Brown, and P. Mojabi, "Toward an end-to-end metasurface design procedure for power pattern synthesis," in *IEEE Int. Symp. Antennas Propag. and USNC-URSI Rad. Sci. Mtg.*, 2021, pp. 617–618.

[14] V. G. Ataloglou and G. V. Eleftheriades, "Arbitrary wave transformations with Huygens' metasurfaces through surface-wave optimization," *IEEE Antennas and Wireless Propagation Letters*, vol. 20, no. 9, pp. 1750–1754, 2021.